J. Biophotonics **9**, No. 9, 948–957 (2016) / **DOI** 10.1002/jbio.201500324

Journal of BIOPHOTONICS

FULL ARTICLE

easySTORM: a robust, lower-cost approach to localisation and TIRF microscopy

Kwasi Kwakwa[*,1], *Alexander Savell*[1,2], *Timothy Davies*[3], *Ian Munro*[1], *Simona Parrinello*[3], *Marco A. Purbhoo*[4], *Chris Dunsby*[**,1,5], *Mark A. A. Neil*[**,1], *and Paul M. W. French*[**,1]

[1] Photonics Group, Physics Department, Imperial College London, London SW7 2AZ
[2] Institute of Chemical Biology, Imperial College London, London SW7 2AZ
[3] MRC Clinical Sciences Centre, Imperial College London, Du Cane Road, London W12 0NN
[4] Section of Hepatology, QEQM Hospital, Imperial College London, London, W2 1PG, UK
[5] Centre for Pathology, Imperial College London, London W12 0NN

Received 11 December 2015, revised 21 January 2016, accepted 31 January 2016
Published online 12 March 2016

Key words: Microscopy, super-resolution, localization, PALM, STORM

TIRF and STORM microscopy are super-resolving fluorescence imaging modalities for which current implementations on standard microscopes can present significant complexity and cost. We present a straightforward and low-cost approach to implement STORM and TIRF taking advantage of multimode optical fibres and multimode diode lasers to provide the required excitation light. Combined with open source software and relatively simple protocols to prepare samples for STORM, including the use of Vectashield for non-TIRF imaging, this approach enables TIRF and STORM imaging of cells labelled with appropriate dyes or expressing suitable fluorescent proteins to become widely accessible at low cost.

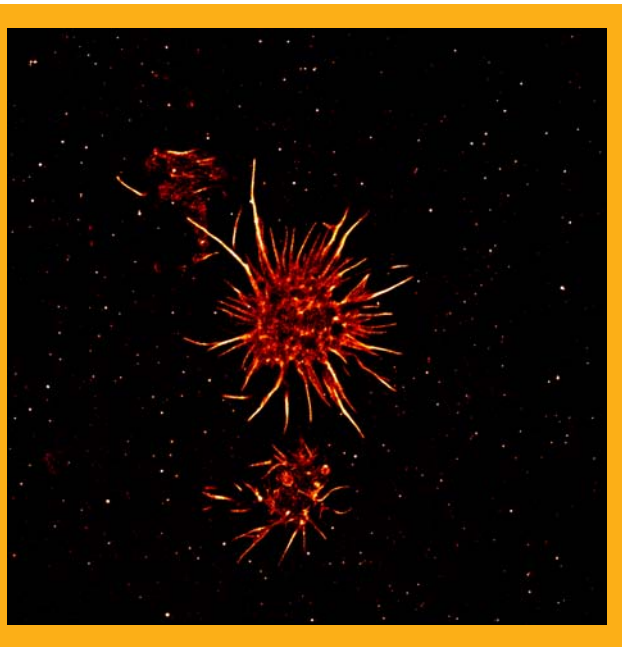

* Corresponding author: e-mail: k.kwakwa@imperial.ac.uk
** These authors contributed equally to this work.

1. Introduction

Super-resolved microscopy (SRM) techniques are becoming widely established through structured illumination approaches [1, 2], stochastically switched single molecule localisation techniques such as PALM [3, 4] and STORM [5], and RESOLFT [6] techniques such as stimulated emission depletion (STED) microscopy [7, 8]. The SRM techniques have transformed cell microscopy in terms of the aspirations of users and have driven significant investments in new microscope technology. After the stunning results presented in the early pioneering papers, there is now an increasing emphasis on making SRM techniques and instrumentation more accessible. Implementing SRM with commercially available instrumentation typically requires complete new microscope systems to be purchased, which are relatively expensive. While STED and SIM require significant engineering of the microscope system and may therefore be best integrated in a bespoke microscope, localisation microscopy can be implemented on existing wide-field or TIRF microscopes [9]. The key components needed to realise STORM or PALM are (i) suitable software for image capture and localisation of switching/blinking fluorophores, (ii) appropriately labelled and mounted samples, (iii) a camera with sufficient imaging speed, sensitivity and dynamic range and (iv) excitation sources of sufficient power. We demonstrate here that an existing wide-field epifluorescence microscope can be adapted for localisation microscopy with components costing less than ~£20,000. We believe this should enable manufacturers to reduce costs and research groups to upgrade existing instruments such that these techniques can be routinely implemented for biological studies and readily combined with other modalities such as electron microscopy for correlative imaging [10] and automated microscopy for high throughput SRM [11].

Since the first demonstrations of PALM and STORM, a wide variety of software tools for localisation microscopy have been produced, many of which are open source. While the choice can be bewildering and it is still not straightforward to compare the different strengths of different software packages – particularly to separate the localisation performance from the image processing and visualisation – it is not difficult to find a software package that provides reasonable results. Reference [12] provides a useful overview of the performance of many of the currently available localisation software packages. We have used the open source ThunderSTORM [13] software for the results presented here.

The optimum sample preparation will depend on the specific modality of localisation microscopy to be used. We have chosen to work with dSTORM [14] approaches because they are conveniently applicable to a wide-range of samples and can be implemented with only a single laser (i.e. radiation at one specific wavelength) to implement excitation and blinking of a chosen fluorophore. Multi-label STORM can then be realised using multiple fluorophore species together with their respective excitation sources [15]. To simplify sample preparation, we have adopted protocols to mount samples for dSTORM in Vectashield [16], which avoids the preparation of complex chemical buffers and the need to use relatively expensive sample chambers in order to contain the liquid buffers.

STORM works particularly well with dye-based labels that offer relatively high brightness and photostability, compared to fluorescent proteins for example. However, while it is possible to chemically modify some dyes to conjugate them to ligands that directly label cellular components such as actin [17], labelling specific target proteins using dyes often requires them to be used in conjunction with antibodies, which typically do not provide the specificity that is achievable with genetically expressed photoswitchable or photoactivatable fluorophores, as are routinely used with PALM and RESOLFT microscopy. Labelling specificity can be improved through the use of genetically expressed (non-fluorescent) tags to which dye labels can be coupled [18–20]. Alternatively, antibodies can be used to conjugate dye labels to genetically expressed fluorescent proteins and thereby "boost" the fluorescence [21]. It is, however, possible to directly implement STORM with fluorescent protein labels such as mCitrine [22] and mCherry [23], and although these are less bright and less photostable than the best STORM dyes, this approach may be the most straightforward to implement for many experiments.

2. Experiments and results

An elegant paper previously describing low-cost STORM microscopy [25] focussed on developing an entire instrument with an impressive balance between performance and cost (below $25,000). However, assembling such a system would require significant technical expertise and the result may not be well-suited for a biology imaging facility. Here we aim to present minor modifications that could be made to existing microscopes to implement STORM while retaining the advantages of instruments optimised for multi-user facilities. The simplest modification we propose is the addition of a laser illuminator to a standard wide-field microscope equipped with a cooled sCMOS camera. This can be conveniently implemented using a multimode optical fibre (MMF) to deliver the excitation light [22]. We note that the use of such an MMF to couple the excitation radiation to the microscope results in higher (>90%)

transmission to the microscope and relatively relaxed tolerances on the alignment of the optical system compared to systems using single mode optical fibres (SMF). In turn, this enables excitation lasers with reduced output power and spatial beam quality to be used. Furthermore, the multimode propagation in an MMF can also help reduce many of the uniformity artefacts seen with coherent illumination by introducing laser speckle that can be time averaged, e.g. by vibrating the optical fibre [9].

Figure 1 shows our configuration in which the excitation laser radiation is coupled into a multimode optical fibre (MMF) connected directly (using an SMA connector) to an achromatic reflective fibre collimator (RFC) unit (Thorlabs, RC12). The collimated excitation beam is focussed into the back focal plane of the objective lens of a standard widefield microscope by lens L2 to provide Köhler illumination over a ~140 µm diameter field of view. The size of the illuminated FOV scales with the numerical aperture (NA) of the delivery fibre or the RFC (NA = 0.216), whichever is smaller, and the extent to which the excitation light is coupled to higher order modes in the fibre. To minimise speckle across the field of view, we can use a vibrator unit (Cairn Research Ltd, P1350/DES/000) oscillating at ~230 Hz, to provide an effectively uniform illumination. Supplementary Figure S2 shows the spatial variation of intensity across the field of view for a range of different MMFs, without and with the fibre vibrator, using excitation radiation at 488 nm from a diode laser (Omicron Luxx).

Figure 2(a, b) show epifluorescence and STORM images of fixed immortalised Human Fibroblast (HFF) cells expressing Lifeact-mCitrine [26], which labels actin, mounted in Vectashield. The use of mCitrine for dSTORM was previously reported in A431 cells expressing mCitrine-erb3 [22] using Mowiol containing DABCO and 50 mM DTT (or 100 mM MEA). Here we present STORM of mCitrine labelled cells mounted in Vectashield for the first time, which further simplifies the sample preparation and relaxes the requirement to handle liquid buffers. These mCitrine dSTORM images were acquired using a single spatial mode diode laser that provided up to 200 mW continuous wave (c.w.) output power at 488 nm. This excitation radiation was delivered to the microscope via a (200 µm core diameter, NA = 0.39) MMF, as depicted in Figure 1.

The most widely used fluorophore label for STORM is Alexa Fluor® 647. Figure 2(d, e) shows epifluorescence and STORM images of a fixed mouse primary brain microvascular endothelial cell with tubulin labelled with Alexa Fluor 647. These cells were embedded in Vectashield to facilitate the fluorophore blinking required for dSTORM. The excitation source was a broad-stripe multimode laser diode (USHIO HL63193MG, commercially available for < $ 50) delivering up to 750 mW at 638 nm that was efficiently (~90%) coupled into the 200 µm core diameter MMF (Thorlabs, M72L05). A standard epifluorescence oil immersion microscope objective (Carl Zeiss, Plan-Apochromat 63×/1.40 NA) was used and, since the excitation laser couples to many modes in the MMF, a uniform illumination was achievable without using the fibre vibrator (see Supplementary Figure S2). We believe that this configuration provides a straightforward, low-cost route to implement 2D STORM on any epifluorescence microscope with unprecedented affordability and simpli-

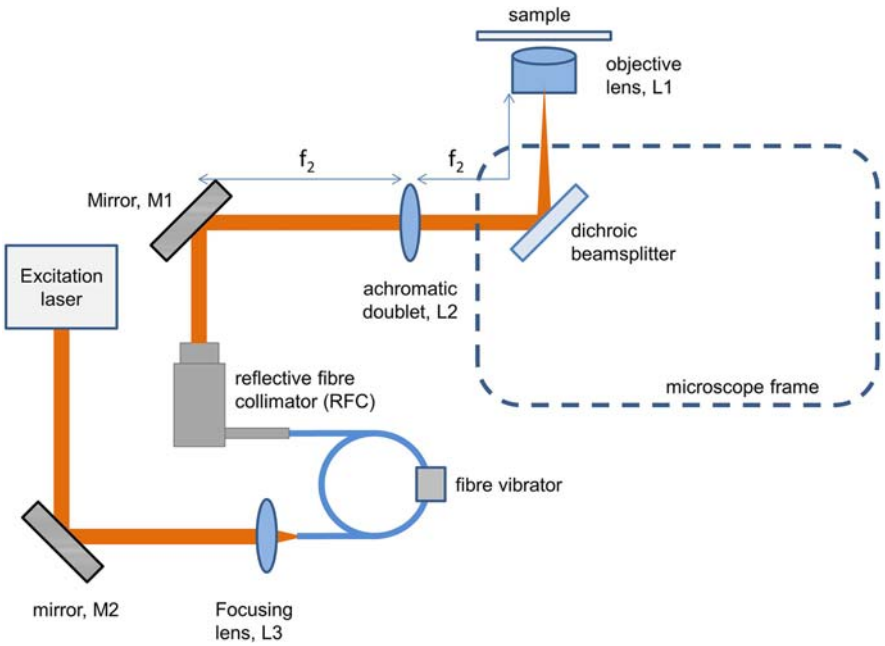

Figure 1 Schematic of experimental set-up for epifluorescence STORM (see Methods section for details).

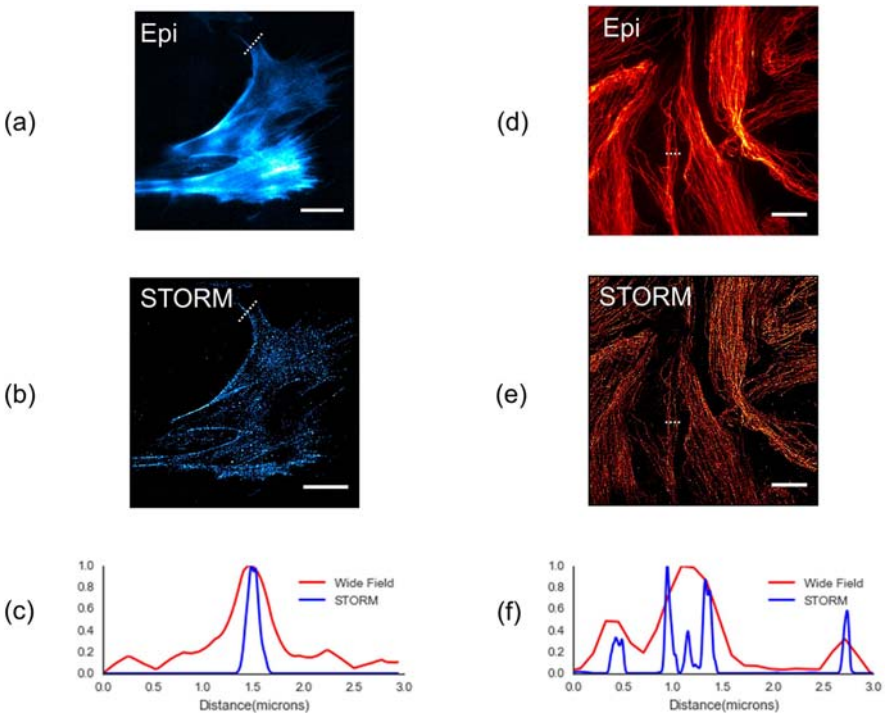

Figure 2 Epifluorescence (**a**, **d**) and STORM (**b**, **e**) images of actin cytoskeleton in fixed HFF cells expressing Lifeact-mCitrine (**a**, **b**) and mouse brain endothelial cells (**d**, **e**) with Alexa Fluor 647 labelling tubulin. (**c**, **f**) show line sections of epifluorescence and STORM images as indicated. Localisation numbers and precisions reported by ThunderSTORM software for (**b**, **e**) were ~25 nm for 410 K localizations and ~15 nm for 2.8 M localizations respectively. Scale bar is 10 µm.

city. Such a simple, alignment-tolerant system would be practical for high throughput automated STORM-based assays, as has been explored using PALM [11] and, with the addition of an appropriate cylindrical lens before the camera, the same system could be modified to implement 3-D STORM [27, 28].

To demonstrate the broader applicability of this approach, we have also demonstrated STORM in Vectashield embedded samples using Alexa Fluor® 555- and Alexa Fluor® 594-labelled mouse primary brain microvascular endothelial cells, achieving localisation precisions of 15 nm and 21 nm respectively for the exemplar images shown in Supplementary Figure 1. These samples were excited using radiation at 561 nm from a single spatial mode solid-state laser source (Cobolt 561 Jive) delivered via the 100 µm core diameter optical fibre.

STORM microscopy is frequently undertaken using total internal reflection fluorescence (TIRF) microscopes that provide ultrathin optical sections

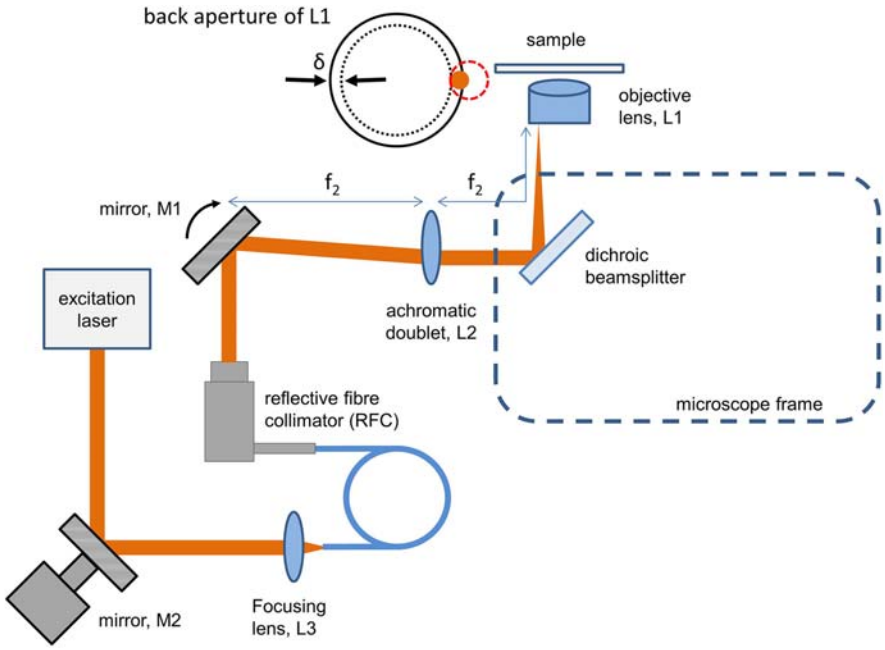

Figure 3 Schematic of experimental set-up for TIRF and TIRF STORM (see Methods section for details) with inset showing excitation light imaged from 50 µm (orange circle) and 100 µm (red dashed line) core diameter onto the back aperture of TIRF objective lens. The positions of the orange circle and red dashed line indicate the positions used for TIRF and δ represents the width of the ring at the perimeter of the back aperture of the objective lens where the bean has to enter for TIRF to be achieved.

near the coverslip and reduced out of focus background, which can improve the localisation. TIRF objectives also typically provide relatively high NA, which additionally improves fluorescence collection efficiency as well as lateral resolution. Commercial TIRF systems typically utilise relatively high power excitation lasers with radiation delivered using single-mode optical fibres (SMF). Here we show that a (50 µm core diameter, NA = 0.22, Thorlabs M42L05) MMF can be used to deliver excitation radiation for TIRF microscopy and TIRF-STORM. Again, this means that alignment tolerances are relaxed and lower power excitation lasers, including multimode diode lasers, can be used for both TIRF and STORM because of the higher coupling efficiency compared to when using SMF.

This can be simply implemented using the optical system depicted in Figure 1 by adjusting the steerable mirror M1 such that the excitation beam is focussed to the periphery of the back aperture of the microscope objective, as illustrated in Figure 3. However, it is important to ensure that the excitation does meet the conditions for TIRF illumination, which is nontrivial when using MMF to deliver the laser radiation.

The radius of the effective limiting aperture in the back focal plane of an aberration-corrected objective obeying Abbe's sine condition is given by $r = f_b$ NA [29] where NA is the numerical aperture of the objective lens and f_b is the back focal length of the objective lens. f_b is given by M/F_{tube}, where M is the magnification of the microscope objective and F_{tube} is the focal length of the standard tube lens.

The condition for TIRF illumination is that the angle of incidence at the coverslip-sample interface should be greater than the critical angle of incidence, $\sin \varphi_c = n_{\text{sample}}/n_{\text{coverslip}}$. This corresponds to the excitation radiation being incident on the objective back aperture at a distance from the optical axis of greater than $f_b\, n_{\text{coverslip}} \sin \varphi_c = f_b\, n_{\text{sample}}$. Thus only excitation radiation focussed within an annulus of width $\delta = f_b$ (NA – n_{sample}) will contribute to the evanescent TIRF excitation. For the microscope used in this study, this is given by $\delta = 1.69\,(1.46 - 1.335)$ mm = 0.21 mm, assuming a refractive index for PBS of ≈1.335. We note that Vectashield, with a refractive index of ∼1.45, cannot be used for mounting samples for TIRF microscopy.

In our set-up, the 50 µm diameter core of the MMF connected to the reflective fibre collimator is imaged to the objective back aperture (Zeiss 100×/1.46 NA) with a magnification of ×5, so most of this radiation will contribute to the TIRF excitation. The excitation light could be adjusted so that the remainder did not provide non-TIRF illumination, i.e. it falls outside the back aperture, as indicated in Figure 3. Figure 4(a, b) shows TIRF and TIRF STORM images respectively of the NK cells with Alexa647-Phalloidin labelling actin acquired using the 638 nm multimode diode laser and the 50 µm core diameter delivery fibre. For comparison Figure 4(d, e) show TIRF and TIRF STORM images acquired using a

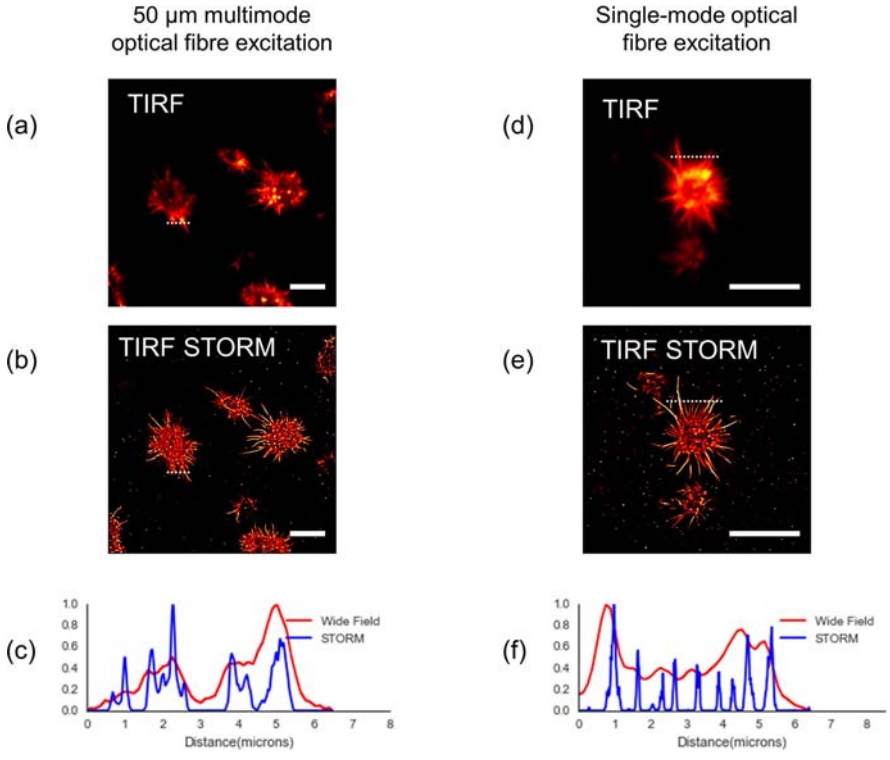

Figure 4 TIRF (**a**, **d**) and TIRF STORM (**b**, **e**) images of actin cytoskeleton in fixed NKL cells with Alexa647 labelling actin mounted in STORM buffer. (**c**, **f**) show line sections of TIRF and TIRF STORM images as indicated. Localisation precision reported by ThunderSTORM software for (**b**, **d**) was ≈15 nm for both images. There were 7.1 M localized molecules for the 50 µm STORM image and 3.2 M for the single mode STORM image. Scale bar is 10 µm. Note that the higher numerical aperture, flatter illumination and increased transmission efficiency of the MMF compared to the SMF enables STORM to be realised over a larger field of view (∼64 µm across for MMF excitation compared to ∼32 µm for SMF excitation).

(NA = 0.14) SMF fibre to deliver excitation radiation from a single spatial mode diode laser (Thorlabs P1-460B-FC-2) providing up to 120 mW output power at 638 nm. Clearly we can also use this TIRF illumination set-up with larger core MMFs, but this will mean that we couple less light into the TIRF evanescent wave and there will therefore be more excitation of fluorescence away from the coverslip. In order to illustrate the optical sectioning achieved using this approach to TIRF microscopy, Supplementary Video 1 shows *z*-stacks of fluorescence images of the same cells acquired with the excitation focussed either on axis (for epi-illumination as in Figure 1) or at the perimeter of the pupil of the objective (as shown in Figure 3) as the microscope was focused at increasing depth into the sample for the SMF and MMF delivery fibres with core diameters ranging from 50 µm to 400 µm using the single spatial mode diode laser at 638 nm. For the 50 µm core delivery fibre with the excitation focussed to the perimeter of the objective lens pupil, TIRF illumination is achieved and there is still significant optical sectioning in the images acquired with the 100 µm delivery fibre. This "TIRF effect" is much less apparent with the larger core diameter fibres.

We can also implement TIRF and TIRF STORM using 50 µm diameter core MMF to deliver excitation radiation from single spatial mode (TEM_{00}) lasers, as shown in Figure 5 where HFF cells with mCitrine-Lifeact labelled actin are excited with the single mode diode laser at 488 nm. For this configuration, it is desirable to time-average the speckle of the illumination pattern, but the fibre vibrator unit does not produce sufficient mode mixing in MMF with core diameters as small as 50 µm. Instead, we rotate mirror M2 about an axis slightly off perpendicular (~1 mrad) to its surface using an electric motor at 4000 rpm. The rotation causes the input laser beam to rapidly scan a circle across the core of the input face of the fibre, thereby launching into a range of different modes and achieving the desired time averaging of the speckle. The (~67 Hz) rotation speed of the mirror is sufficient for the 20–40 Hz image acquisition rates of these experiments but may need to be increased if higher frame rate acquisitions are required. A similar approach can be implemented with a rotating optical wedge [30] or a transparent component that is not optically flat, such as plastic petri dish [31], but simply rotating one of the laser beam steering mirrors provides the required despeckling with lower insertion loss. This approach is also applicable to larger core MMFs where it can replace the fibre vibrator as the mode-mixing device, as illustrated in Supplementary Figure 2. The comparison between fluorescence *z*-stacks acquired with the excitation radiation focussed on axis and at the objective lens perimeter using different delivery fibres using the rotating mirror to reduce speckle in the illumination is presented in Supplementary video 2.

This robust and low cost approach to implementing TIRF microscopy and TIRF STORM can be extended to multilabel imaging, as illustrated in Figure 6, which presents an exemplar biological applica-

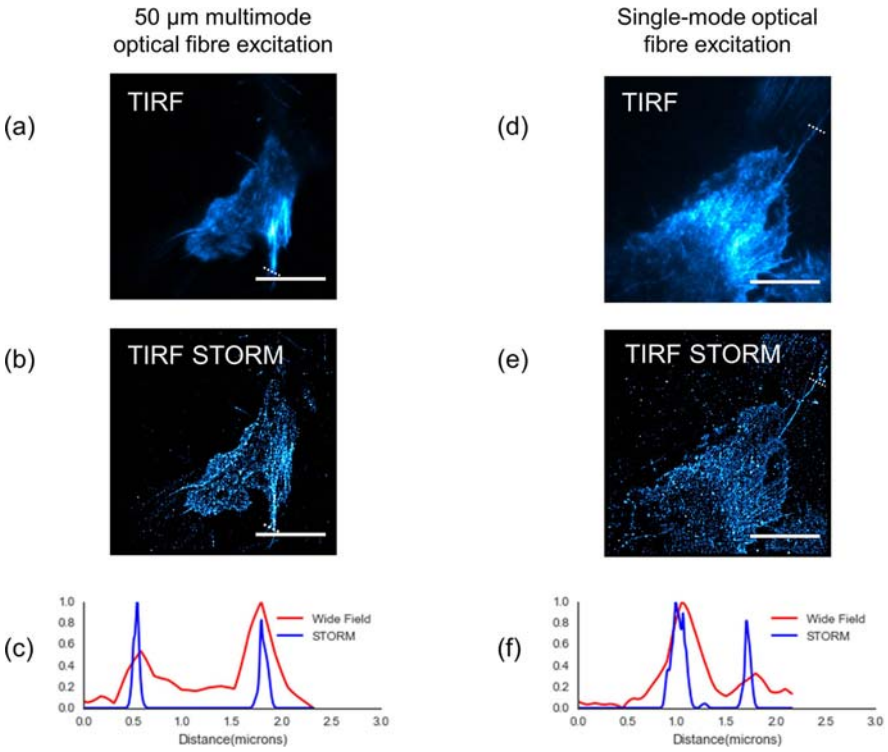

Figure 5 TIRF (**a**, **d**) and TIRF STORM (**b**, **e**) images of actin cytoskeleton in fixed HFF cells expressing Lifeact-mCitrine mounted in STORM buffer. (**c**, **f**) show line sections of TIRF and TIRF STORM images as indicated. Localisation precision and numbers reported by ThunderSTORM software for (**b**, **d**) was ≈25 nm and ≈300 K molecules for both images. Scale bar is 10 µm.

tion where ATTO 488-Phalloidin (excited at 488 nm) and SiR-Tubulin (excited at 638 nm) have been used to label actin and tubulin respectively in NKL cells forming an artificial "immunological synapse" (IS) with a layer of activating ligand. This artificial IS approach has previously been used, e.g. [32], for studies of signalling and cytoskeletal changes associated with the immunological synapse. Although there is scope for optimising the labelling and imaging protocol, these first results are encouraging and this STORM methodology will form the basis of future work to elucidate the interactions of actin and tubulin at the IS.

3. Methods and materials

3.1 Cell culture and sample preparation

The NK cell lymphoma cell line, NKL, and the Human Foreskin Fibroblast Cell line, HFF, were used. The HFF cells stably expressed a construct of the Lifeact peptide, which stains filamentous actin C-terminally tagged with mCitrine. Both cell lines were cultured in RPMI 1640 Media containing 10% FBS (GIBCO). NKLs were supplemented with 100 U/ml Human IL-2 (Roche). For imaging in liquid buffers, Lab-Tek II 8-well chambered coverslips (#1.5) washed with 96% ethanol and air-dried were used. For imaging in Vectashield, samples were mounted on #1.5 borosilicate glass coverslips washed with 96% ethanol and dried with lens tissue.

For the single-labelled NKL samples, the coverslips were then coated with 1 mL 0.01% Poly-l-lysine for 20 minutes prior to removal and air-dried, while for the HFF samples, coverslips were coated with 200 μM fibronectin solution and incubated for one hour at 37 °C. All samples were washed twice with PBS and once in RPMI media containing 5 mM HEPES before approximately 100,000 cells re-suspended in 200 μL of HEPES media were incubated for 30 minutes (NKL) or overnight (HFF-LA-mCitrine) on the slips at 37 °C. Cells were fixed for 20 minutes in 4% methanol free paraformaldehyde and permeabilised for 4 minutes with 0.1% Tryton X. At this stage the HFF cells were washed in PBS three times and kept under PBS until imaging. The NKL cells were blocked for 1 hr using 5% BSA and then stained using 5 μL Alexa647-Phalloidin per slide in 5% BSA (final dye concentration ~165 nM) for 90 minutes. These were then also washed in PBS three times and kept under PBS until imaging.

For STORM imaging in Vectashield, a solution of 1 part Vectashield in 6 parts Glycerol with 50 mM pH8 TRIS-buffer was spotted onto microscope slides. PBS was removed from the samples on the coverslips and the coverslips were placed on the microscope slides to mount the samples in the Vectashield preparation. Excess mounting media was removed with tissue before sealing the slides with commercial nail varnish.

For TIRF STORM imaging in lower refractive index (liquid) buffers, the PBS was removed and 1 mL of imaging buffer was added. For the HFF

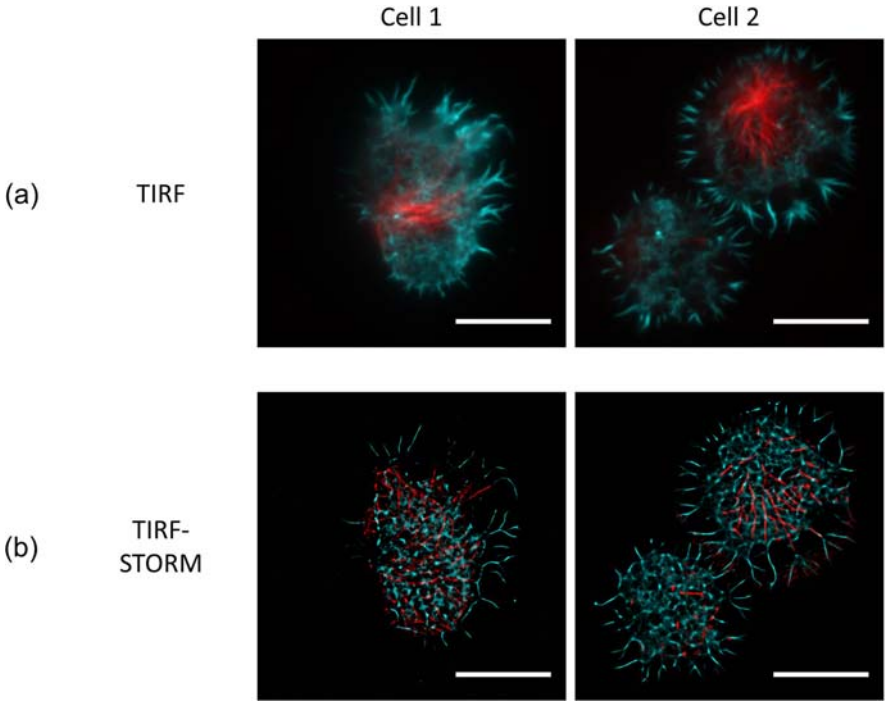

Figure 6 TIRF (**a**) and TIRF STORM (**b**) images of dual labelled NKL cells on a coverslip coated with activatory NKG2D antibody to form an immunological synapse with ATTO488-Phalloidin (blue) labelling actin and SiR-Tubulin (red) labelling tubulin. Localisation precision reported by ThunderSTORM software was 18 nm for actin (3 M localizations for cell 1, 5.6 M localizations for cell 2) and 16 nm for tubulin images (900K localizations for cell 1, 1.2 M for cell 2). Scale bar is 10 μm.

cells, a simple buffer of 100 mM MEA in PBS was used. For the NKL cells, 40 μg/mL Catalase, 500 μg/mL Glucose Oxidase and 10% (w/v) Glucose was added to the buffer comprising 100 mM MEA in PBS.

For the double-labelled imaging of actin and tubulin at the artificial immunological synapse shown in Figure 6, Poly-l-lysine coated slides (as previously) were incubated overnight at 40° with 3 μM activating ligand (Human NKG2D/CD314 Antibody, R&D Systems MAB139) before being washed and seeded with NKL cells. These cells were washed 3 times in PBS before being fixed at room temperature for 30 minutes using 10 mM EGS in 10% DMSO solution. The reaction was quenched for 15 minutes using full RPMI 1640 culture media containing 5 mM HEPES Buffer. The cells were then permeabilised, blocked and stained with SiR-Tubulin and Atto488-Phalloidin as described above before imaging under the STORM buffer.

For the images presented in Figure 2(d, e) and Supplementary Figure 1, mouse primary brain microvascular endothelial cells were plated on PLL coated coverslips coated with laminin for 30 minutes at 37 °C. Cells were then fixed in 4% PFA for 15 minutes at room temperature and blocked with 3% BSA in PBS for 30 minutes at room temperature. Tubulin was labelled using a 1 : 500 dilution of mouse anti-B tubulin (Sigma, ST5293) in blocking buffer for two hours at room temperature. Following washing cells were incubated in 1 : 400 Alexa 555/Alexa594 in blocking buffer for 1 hour at room temperature. Cells were then mounted in 1 : 6 solution of Vectashield: 50 mM TRIS pH8.

3.2 Microscope configuration

Excitation at 488 nm was realised by a single spatial mode laser diode (Omicron Luxx) providing up to 200 mW output power. For the images shown in Supplementary Figure 1, excitation at 561 nm was realised by a single spatial mode solid-state laser (Cobolt 561 Jive) able to provide up to 200 mW output power. When using these lasers with MMF to deliver the excitation radiation, a telescope comprising two singlet lenses was used to expand the beam by 7.5× and then a 30 mm focal length achromatic doublet lens (L3 in Figure 3) was used to focus the single spatial mode laser radiation into the MMF. The diameter of the expanded 488 nm beam incident at lens L3 was ∼8 mm and so the NA of the focussed light was ∼0.13. One of the steering mirrors (M2) was mounted such that it could be rotated using an electric motor in order to time-average the speckle, as discussed in the main text. This mirror was located 200 mm from lens L3 (see Figure 3) focussing the light into the optical fibre. The same optical set-up (with static steering mirror M2) was used to couple the laser radiation into the SMF.

Excitation at 638 nm was provided by a multimode broad stripe laser diode providing up to 700 mW (USHIO HL63193MG) from a 40 μm wide facet, which was mounted in a temperature controlled laser diode mount (Thorlabs, TCLDM9). A 4.6 mm focal length aspheric lens (Thorlabs, C230TMD-A) was used to approximately collimate the laser diode emission parallel to the diode stripe such that the beam slowly diverged in the plane perpendicular to the diode stripe. The beam was then focused by the 30 mm focal length achromatic doublet lens (Thorlabs, AC254-030-A-ML) into the MMF. The diameter of this 638 nm beam incident at lens L3 (see Figure 3) was ∼12 mm and so the NA of the focussed light was ∼0.2. The same optical set-up (with static steering mirror M2) was used to couple light the laser radiation into the SMF.

The delivery optical fibres were connected to an achromatic reflective fibre collimator (Thorlabs, RC12FC-P01) of 50.8 mm focal length and 0.216 NA and the collimated excitation beam was focused into the back aperture of the objective lens of an inverted fluorescence microscope (Carl Zeiss, Axio Observer) using an achromatic doublet of 250 mm focal length (ThorlabsAC254-250-A-ML). Fluorescence images were acquired using a sCMOS camera (Hamamatsu Orca 4.0v2) in rolling shutter mode set to 2 × 2 binning of the camera's pixels to yield a lateral effective pixel size of 126 nm. The microscope, camera and 488 nm excitation laser were all controlled during image acquisition using the Micro-Manager software.

3.3 STORM protocol

Once the sample had been brought into focus, the drift correction module on the microscope was engaged and the excitation laser power was increased until stochastic blinking was observed (typically at ∼0.5–5 kW/cm^2). Between 10,000 and 20,000 frames were acquired for each field of view with frame exposure times of 20 ms, 30 ms and 40 ms for the samples labelled with the SiR dye, Alexa dyes and mCitrine respectively. The acquired images were processed to determine fluorophore localisation, the localisations were then filtered by localisation uncertainty and the final image was visualized all using the open source ThunderSTORM software [12]. Lateral drift in the sample during the STORM data acquisition was corrected for using a cross-correlation of the particle locations using the drift-correct option in ThunderSTORM. Drift observed between the STORM and non-STORM images was

corrected using image correlation to determine the required correction.

The raw data and STORM images are saved to an OMERO [24] image data server as OME-TIFF files and these, together with the localisation data and reconstructed STORM images underlying the figures presented here will be publically available at: https://cisbic.bioinformatics.ic.ac.uk/omero/webclient/?show=project-4116

4. Discussion

In conclusion, we have demonstrated low-cost and simple optical configurations for realising STORM and TIRF microscopy that can be implemented on standard wide-field microscopes. Where TIRF is not required, the use of multimode diode laser excitation sources and MMF optical fibres provides a simple approach to realising STORM in a standard wide-field epifluorescence microscope. If single spatial mode laser excitation sources are to be used, then the use of a fibre vibrator or rotating steering mirror can time-average the illumination field to suppress speckle when radiation is delivered by MMF. Where TIRF is required, this can be implemented on a standard wide-field microscope by using a TIRF objective and delivering the excitation light with a 50 μm core diameter MMF. When using fluorophores excited in the red, low-cost multimode diode lasers are available that can couple efficiently to such MMF fibres. The combination of a multimode laser diode and MMF is advantageous compared to using single spatial mode lasers since it reduces the speckle and enables a particularly simple and cost-effective simple implementation of TIRF and STORM – see Supplementary Table 1 for approximate costing. Excitation at shorter wavelengths can be provided using low-cost diode lasers or diode-pumped solid-state lasers, noting that the use of MMF delivery fibres can significantly reduce the cost of excitation lasers (since the delivery efficiency is much higher than for SMF) and of the fibre launch systems (since the requirements for mechanical precision and stability are relaxed). We also note that the imaging of the MMF to the back focal plane of the objective can be easily modified to change the field of view and the corresponding excitation intensity to optimise STORM for a given excitation power – and the higher intensities achievable using MMF delivery of excitation radiation can enable STORM over larger fields of view compared to when using SMF. The simple rotation of a laser beam steering mirror directing laser radiation to a MMF provides a cost effective approach to time-average speckle in the illumination field. This could be implemented generally in epifluorescence microscopes and other applications where speckle-free wide-field laser illumination is required, noting that this is generally challenging to achieve at low cost and low insertion loss.

These straightforward optical configurations for STORM microscopy, particularly using low-cost multimode diode lasers at 638 nm and MMF to deliver the excitation radiation, can be combined with open source software for localisation and image processing and can be applied with relatively simple techniques for sample preparation, notably using Vectashield with standard coverslips and microscope slides rather than using liquid buffers in imaging wells. This low-cost "easySTORM" approach could be extended to multilabel SRM as broad-stripe multimode diode lasers become available at other wavelengths. To the best of our knowledge this is the first report of STORM using of Alexa 594 and mCitrine in Vectashield. We believe there is considerable scope for further optimisation of protocols for simple and robust preparation of samples for STORM microscopy – particularly to optimise multilabel imaging. Thus we believe the methodologies reported here, will aid researchers assembling their own TIRF and STORM microscopes and hopefully help manufacturers to provide lower cost commercial instrumentation.

Supporting Information

Additional supporting information can be found in the online version of this article at the publisher's website.

Acknowledgements The authors gratefully acknowledge funding from the UK Medical Research Council (MRC, MR/K015834/1 and MC_A652_SPz10), the Biotechnology and Biological Sciences Research Council (BBSRC, BB/M018423/1) and the Wellcome Trust (WT093465MA and WT095931/Z/11/Z). Alex Savell acknowledges a PhD studentship from the Institute of Chemical Biology Doctoral Training Centre funded by the UK Engineering and Physical Science Research Council (EPSRC).

References

[1] M. G. L. Gustaffsson, J. Microscopy **198**, 82–87 (2000).
[2] M. G. L. Gustaffsson, Proc. Natl. Acad. Sci. U.S.A. **102**, 13081–13086 (2005).
[3] E. Betzig, G. H. Patterson, R. Sougrat, O. W. Lindwasser, S. Olenych, J. S. Bonifacino, M. W. Davidson, J. Lippincott-Schwartz, and H. F. Hess, Science **313**, 1642–1645 (2006).
[4] S. T. Hess, T. P. Girirajan, and M. D. Mason, Biophys. J. **91**, 4258–4272 (2006).

[5] M. J. Rust, M. Bates, and X. Zhuang, Nat. Methods **3**, 793–796 (2006).
[6] M. Hofmann, C. Eggeling, S. Jakobs, and S. W. Hell, Proc. Natl. Acad. Sci. U.S.A. **102**, 17565–17569 (2005).
[7] S. W. Hell and J. Wichmann, Opt. Lett. **19**, 780–782 (1994).
[8] T. A. Klar, S. Jakobs, M. Dyba, A. Egner, and S. W. Hell, Proc. Natl. Acad. Sci. U.S.A. **97**, 8206–8210 (2000).
[9] P. Almada, S. Culley, and R. Henriques, Methods (2015) advance publication: http://dx.doi.org/10.1016/j.ymeth.2015.06.004.
[10] S. Watanabe, A. Punge, G. Hollopeter, K. I. Willig, R. J. Hobson, M. W. Davis, S. W. Hell, and E. M. Jorgensen, Nat. Methods **8**, 80–84 (2011).
[11] S. J. Holden, T. Pengo, K. L. Meibom, C. Fernandez-Fernandez, J. Collier, and S. Manley, Proc. Natl. Acad. Sci. **111**, 4566–4571 (2014).
[12] D. Sage, H. Kirshner, T. Pengo, N. Stuurman, J. Min, S. Manley, and M. Unser, Nat. Methods **12**, 717–724 (2015).
[13] M. Ovesny, P. Krizek, J. Borkovec, Z. Svindrych, and G. M. Hagen, Bioinformatics **30**, 2389–2390 (2014).
[14] J. Fölling, M. Bossi, H. Bock, R. Medda, C. A. Wurm, B. Hein, S. Jakobs, C. Eggeling, and S. W. Hell, Nature Methods **5**, 943–945 (2008).
[15] M. Bossi, J. Föiling, V. N. Belov, V. P. Boyarskiy, R. Medda, A. Egner, C. Eggeling, A. Schönle, and S. W. Hell, Nano Lett. **8**, 2463–2468 (2008).
[16] N. Olivier, D. Keller, V. S. Rajan, P. Gönczy, and S. Manley, Biomed. Opt. Express **4**, 885–899 (2013).
[17] G. Lukinavičius, L. Reymond, E. D'Este, A. Masharina, F. Göttfert, H. Ta, A. Güther, M. Fournier, S. Rizzo, H. Waldmann, C. Blaukopf, C. Sommer, D. W. Gerlich, H.-D. Arndt, S. W. Hell, and K. Johnsson, Nat. Methods **11**, 731–733 (2014).
[18] K. Kolberg, C. Puettmann, A. Pardo, J. Fitting, and S. Barth, Curr. Pharm. Des. **19**, 5406–5413 (2013).
[19] G. V. Los, L. P. Encell, M. G. McDougall, D. D. Hartzell, N. Karassina, C. Zimprich, M. G. Wood, R. Learish, R. F. Ohana, M. Urh, D. Simpson, J. Mendez, K. Zimmerman, P. Otto, G. Vidugiris, J. Zhu, A. Darzins, D. H. Klaubert, R. F. Bulleit, and K. V. Wood, ACS Chem. Biol. **3**, 373–382 (2008).
[20] J. B. Grimm, B. P. English, J. Chen, J. P. Slaughter, Z. Zhang, A. Revyakin, R. Patel, J. J. Macklin, D. Normanno, R. H. Singer, T. Lionnet, and L. D. Lavis, Nat. Methods **12**, 244–250 (2015).
[21] J. Ries, C. Kaplan, E. Platonova, H. Eghlidi, and H. Ewers, Nature Methods **9**, 582–584 (2012).
[22] P. Křížek, I. Raška, and G. M. Hagen, Opt. Express **19**, 3226–3235 (2011).
[23] C. M. Winterflood and H. Ewers, ChemPhysChem. **15**, 3447–3451 (2014).
[24] http://www.openmicroscopy.org/site/products/omero
[25] T. Holm, T. Klein, A. Lçschberger, T. Klamp, G. Wiebusch, S. van de Linde, and M. Sauer, ChemPhysChem. **15**, 651–654 (2014).
[26] J. Riedl, A. H. Crevenna, K. Kessenbrock, J. H. Yu, D. Neukirchen, M. Bista, F. Bradke, D. Jenne, T. A. Holak, Z. Werb, M. Sixt, and R. Wedlich-Soldner, Nat. Methods **5**, 605–607 (2008).
[27] H. P. Kao and A. S. Verkman, Biophys. J. **67**, 1291–1300 (1994).
[28] B. Huang, W. Wang, M. Bates, and X. Zhuang, Science **319**, 810–813 (2008).
[29] R. Juskaitis, Chapter 11 in Pawley, Handbook Of Biological Confocal Microscopy (2006).
[30] A. L. Mattheyses, K. Shaw, and D. Axelrod, Microsc. Res. Tech. **69**, 642–647 (2006).
[31] J. R. Kuhn and T. D. Pollard, Biophysical Journal **88**, 1387–1402 (2005).
[32] M. A. Purbhoo, H. B. Liu, S. Oddos, D. M. Owen, M. A. A. Neil, S. V. Pageon, P. M. W. French, C. E. Rudd, and D. M. Davis, Science Signaling **3**, 36 (2010).